

The Astrophysical Journal, in press

Detection of the Neupert Effect in the Corona of an RS CVn Binary System by *XMM-Newton* and the VLA

Manuel Güdel, Marc Audard, Kester W. Smith¹

Paul Scherrer Institut, Würenlingen und Villigen, CH-5232 Villigen PSI, Switzerland

guedel@astro.phys.ethz.ch, audard@astro.phys.ethz.ch,
kester@astro.phys.ethz.ch

Ehud Behar

*Columbia Astrophysics Laboratory, Columbia University, 550 West 120th Street, New York,
NY 10027, USA*

behar@astro.columbia.edu

Anthony J. Beasley

*Owens Valley Radio Observatory, California Institute of Technology, Big Pine, CA 93513,
USA*

tbeasley@ovro.caltech.edu

and

Rolf Mewe

*SRON National Institute for Space Research, Sorbonnelaan 2, 3584 CA Utrecht, The
Netherlands*

r.mewe@sron.nl

¹Also Institut für Astronomie, ETH Zentrum, CH-8092 Zürich, Switzerland

ABSTRACT

The RS CVn-type binary σ Geminorum was observed during a large, long-duration flare simultaneously with *XMM-Newton* and the VLA. The light curves show a characteristic time dependence that is compatible with the Neupert effect observed in solar flares: The time derivative of the X-ray light curve resembles the radio light curve. This observation can be interpreted in terms of a standard flare scenario in which accelerated coronal electrons reach the chromosphere where they heat the cool plasma and induce chromospheric evaporation. Such a scenario can only hold if the amount of energy in the fast electrons is sufficient to explain the X-ray radiative losses. We present a plausibility analysis that supports the chromospheric evaporation model.

Subject headings: radio continuum: stars — stars: flare — stars: activity — stars: coronae — stars: individual (σ Gem) — X-rays: stars

1. Introduction

There is compelling evidence that high-energy processes and high-energy particles play a pivotal role in the energy release, energy transport, and plasma heating during solar flares (see review by Hudson & Ryan 1995). A standard scenario proposes that electrons (perhaps also ions) are accelerated in the corona in the course of magnetic reconnection. As the electrons travel along closed magnetic fields, those with large pitch angles and sufficient energy (typically several 100 keV) lose a small part of their energy as gyrosynchrotron radio emission. The bulk kinetic energy of the accelerated electrons, however, is carried to the chromosphere where it is deposited by electron-ion collisions. The collision of the beam with the dense plasma reveals itself by non-thermal hard X-ray radiation (HXR, typically between 10–100 keV) that, however, constitutes only a small fraction ($\sim 10^{-5}$) of the total energy loss. The bulk energy is transformed into heat, producing an overpressure in the chromosphere as the gas cannot radiate away the energy influx sufficiently rapidly. As a consequence, the gas evaporates explosively into the corona as a $\sim 10^7$ K plasma visible in X-rays during the gradual phase of a solar flare (Dennis 1988). The observed gyrosynchrotron radio luminosity L_R and the hard X-ray luminosity L_{HXR} are, to first order, proportional to the instantaneous number of fast electrons and therefore to the power \dot{E} injected into the system, while the slowly variable soft X-ray luminosity L_X is roughly proportional to the accumulated total energy E in the hot coronal flare plasma. One therefore expects that

$$\frac{d}{dt}L_X(t) \propto L_{\text{HXR}}(t) \propto L_R(t), \quad (1)$$

a relation that is commonly known as the ‘Neupert Effect’ (Neupert 1968; Dennis & Zarro 1993). Although significant deviations from this scenario have been observed in solar flares (e.g., heating starting before any hard X-rays can be detected, or absence of one of the emission types discussed above), there is strong support for several features of this model in the majority of solar flares (Dennis & Zarro 1993). For example, the coincidence to within a fraction of a second of HXR brightenings at a pair of magnetic loop footpoints that are separated by $\sim 10^9$ cm requires non-thermal particle velocities (Sakao 1994).

It is thought that the same mechanisms should operate in stellar flares, although flares on some classes of stars deviate considerably from the proposed solar analogy. In particular, giant flares on RS CVn-type binaries may require mechanisms unknown on the Sun. RS CVn binaries, commonly consisting of a giant or subgiant primary with a main-sequence or subgiant companion in a close orbit, are sources of luminous radio and X-ray emission (Drake, Simon, & Linsky 1989). Very long flare time scales and radio source sizes of order of the intrabinary distance have been modeled in terms of giant dipole-like magnetospheric structures (Morris, Mutel, & Su 1990; Jones et al. 1994) into which high-energy particles are injected from a flare site (Mutel et al. 1985), and where they lose most of their energy by radiation. Coordinated observations in X-rays and radio are required to study the importance of high-energy electrons in the heating mechanism. Hawley et al. (1995) reported a Neupert effect-like behavior during a large flare on the dMe star AD Leo, where optical (U band) and EUV emissions were used as proxies for the radiation from high-energy electrons (radio, HXR) and from the thermal plasma, respectively. Güdel et al. (1996) discussed the first stellar Neupert effect seen in the radio and X-ray bands on the dM5.5e binary UV Cet, finding similar timing and similar energy budgets as in solar gradual (“type C”) events.

2. Observations and Data Analysis

σ Gem is a close binary of the RS CVn type, consisting of a K1 III giant and a fainter companion whose spectral classification is unclear (Strassmeier et al. 1993). Its distance is 37.5 ± 1 pc (ESA 1997). It is a luminous radio ($\log L_R \approx 15.40$, in $\text{erg s}^{-1} \text{Hz}^{-1}$; Drake et al. 1989) and X-ray source ($\log L_X \approx 31.0 \pm 0.2$, in erg s^{-1} , Yi et al. 1997 and references therein, all luminosities corrected to the Hipparcos distance), and was monitored previously during flares or during quiescence at radio, EUV, and X-ray wavelengths (Engvold et al. 1988; Pallavicini, Willson, & Lang 1985; Singh et al. 1987; Drake et al. 1989; Schrijver et al. 1995; Yi et al. 1997; Osten & Brown 1999). It is generally assumed that the coronal emission is largely related to the K1 III star.

We observed σ Gem with *XMM-Newton* (Jansen et al. 2001) between 2001 April 6,

16:46 UT – April 7, 07:53 UT, using all five X-ray detectors on board. Since here we are predominantly interested in the time behavior, we will present exclusively the sensitive European Photon Imaging Camera (EPIC) PN light curve for the energy range [0.15, 10] keV (Strüder et al. 2001). The PN camera was operated in the small window mode given the expected brightness of the target (both at optical and at X-ray wavelengths). Background subtraction is irrelevant for the very high source count rate. The features in the light curve were confirmed from the other detectors. The data were processed using the standard SAS software (version of 2001 May). Dead-time corrections were applied (29% of the counts are lost in the utilized mode). For most of the observing time (April 6, 20:12 UT – April 7, 07:58 UT), the Very Large Array (VLA) monitored the 6 cm flux (frequency $\nu = 5 \times 10^9$ Hz) of σ Gem in both left- and right-hand polarizations over a bandwidth of 100 MHz. The calibration of the radio data followed standard procedures within the AIPS software. Individual maps were made for each observing scan ($\approx 12.5'$); the fluxes were read from these maps using the JMFIT task.

3. Results

XMM-Newton observed σ Gem in the course of a large X-ray flare, with a PN peak count rate of ~ 100 cts s^{-1} , corresponding to a luminosity of $\sim 5 \times 10^{31}$ erg s^{-1} or ≈ 5 times the usual quiescent X-ray emission level (as cited above). Figure 1a (top panel) presents the PN light curve, binned to 500 s. Only the peak of this flare was observed. From the PN spectrum, the X-ray emission can be interpreted as being due to hot (several keV), thermal plasma. The simultaneous radio emission (bottom panel in Figure 1) is strongly varying around a few mJy ($= 10^{-26}$ erg cm^{-2} Hz^{-1}), typically on time scales of less than 5000 s. We will concentrate our discussion on the second flare that is fully visible at radio wavelengths, i.e., the episode between 1.03–1.32 d.

Motivated by equation 1, we smoothed the X-ray light curve, either using a boxcar of width 11 bins (equivalent to 5500 s, not shown), or a Chebychev-polynomial fit of order 9 (Figure 1a). We then calculated the time derivative of each smoothed light curve. The results are illustrated in Figure 1b (solid: for Chebychev fit; dotted: for boxcar-smoothed fit), and are to be compared with the radio light curve in panel c. The curves are very similar, signifying a relation close to that described by equation 1, i.e., a Neupert effect. To quantify the relative timing of the two curves, we computed the cross correlation function

as follows:

$$P(\ell) = \frac{m}{m - |\ell|} \frac{\sum_{k=1}^{m-\ell} (R_k - \bar{R})(D_{k+\ell} - \bar{D})}{\left(\left[\sum_{k=1}^m (R_k - \bar{R})^2 \right] \left[\sum_{k=1}^m (D_k - \bar{D})^2 \right] \right)^{1/2}} \quad (2)$$

for a time lag $\ell \geq 0$ in units of bins, where we used $m = 46$ time bins of 500 s each as shown in Figure 1b, for the time interval marked by a horizontal bar in Figure 1c. For $\ell < 0$, D and R are interchanged. Here, R_k is the radio flux and D_k is the X-ray time derivative at the grid point k (the boxcar-smoothed version was used; the result using the Chebychev-smoothed version is in full agreement). The quantities \bar{R} and \bar{D} are the means of the respective variables. The first factor on the right-hand side of equation 2 corrects for the decreasing number of terms in the denominator of the second factor. To obtain identical time bins for both curves, we linearly interpolated the radio data to the grid defined by the X-ray bins; this is sufficiently accurate given the short time bins compared to the intrinsic light curve variability time scales. The inset in Figure 1c shows $P(\ell)$. The function sharply peaks at zero lag, indicating no significant lag between the two curves. Note that the units of the X-ray time derivative and the radio flux are not important for equation 1 and the figures have been scaled arbitrarily. Also, the X-ray time derivative is mostly negative since the variability occurs during the gradual decline from the main peak. Again, this is of little importance as such a trend can be subtracted from the data, shifting the derivative to larger values.

4. Discussion

Figure 1 shows compelling evidence for the presence of a Neupert effect, i.e., a radio light curve that is approximately proportional to the time derivative of the X-ray light curve. The light curves alone do not prove the operation of chromospheric evaporation induced by electron beams. It is possible that the rate of electron injection is proportional to the rate of heating, both being induced by the same mechanism, while the two processes are causally unrelated. A causal relation is difficult to demonstrate even in the case of the Sun, although the evidence for electron beam heating in many solar flares is compelling.

A causal relation between particle acceleration and coronal heating is however supported if the energy in the non-thermal electrons is sufficient to heat the observed plasma. Further, this energy should not be radiated away by the high-energy particles but be transported to the chromosphere on time scales shorter than the radiative loss time. An accurate calculation requires information that is not at hand, but we present estimates for a plausibility analysis

as follows: By estimating the gyrosynchrotron radio flux and assuming reasonable magnetic field strengths and electron distributions, we infer the total kinetic energy in the electrons at any given time. By integrating the energy across the flare, we can compare the total injected energy with the total X-ray losses. For such an order-of-magnitude estimate, we will assume that the shape of the electron distribution stays constant (see below), and that variable radio self-absorption is not relevant. We perform the estimates for a range of given but, in each case, constant values of the magnetic field strength and of the slope of the electron distribution.

Non-thermal electrons in stellar coronae and solar flares are usually distributed in energy in a power law of the form

$$n(E, t) = \frac{N(t)(\delta - 1)}{E_0} \left(\frac{E}{E_0} \right)^{-\delta} \quad (3)$$

where $n(E, t)dE$ is the time-dependent number density of electrons in the energy interval $[E, E + dE]$, E_0 is the lower cutoff energy for the distribution of non-thermal electrons, $N(t)$ is the normalization constant, *viz.* the volumetric number density of electrons at time t above E_0 , and $\delta > 1$ is the power-law index (typically $\delta = 3 - 5$ in solar flares, Dennis 1988). In solar flares, there is evidence that one and the same electron power-law distribution comprises the (lower-energy) hard-X-ray emitting electrons and the (higher-energy) microwave-emitting electrons (Bastian, Benz, & Gary 1998). The value of E_0 is unknown but must be > 0 in order to confine the total non-thermal energy (Dennis 1988). We set $E_0 = 10$ keV. This is likely to be a lower limit for solar flares where $E_0 = 20 - 30$ keV may be more appropriate (Dennis 1988).

Radio flare emission from RS CVn binaries at 5 GHz is often optically thick (Mutel et al. 1985; White & Franciosini 1995). Optically thick emission from a simple source should stay constant, independent of the number of injected electrons, but this is not usually observed (Morris et al. 1990), indicating that the number of electrons itself is responsible for continually changing the optically thick cross section, *e.g.*, by being injected in a variable number of magnetic loops. We will thus assume that the volume filled by non-thermal electrons is generally time-dependent.

The radio spectral index at optically thick low frequencies is typically $+1$, while the index on the high-frequency optically thin side is between -0.5 and -1 (Feldman et al. 1978; Morris et al. 1990; Jones et al. 1996; Beasley et al. 2002). The turnover frequency (above which the radiation changes to optically thin) is similar in many reported flares, $\nu_{\text{peak}} \approx 10 - 20$ GHz although values as low as a few GHz are possible (Morris et al. 1990). From this typical spectral model shape, we can estimate the unabsorbed luminosity at 5 GHz to be $\sim 1 - 10$ times higher than measured. The unabsorbed radio flux f_R (taken to be 5

times the observed flux in what follows) relates to the gyrosynchrotron emissivity η , for which Dulk & Marsh (1982) gave the following approximation for the magnetoionic x-mode:

$$\eta_x = 3.3 \times 10^{-24} 10^{-0.52\delta} B N (\sin\theta)^{-0.43+0.65\delta} \left(\frac{\nu}{\nu_B} \right)^{1.22-0.90\delta} \quad (4)$$

(in $\text{erg cm}^{-3} \text{ s}^{-1} \text{ Hz}^{-1} \text{ sr}^{-1}$). B (in units of Gauss) is the magnetic field strength (assumed to be constant in the source), and $\nu_B \approx 2.8 \times 10^6 B$ [Hz] is the electron gyrofrequency. We will use $\eta = 2\eta_x$ for the total emissivity, assuming a similar emissivity for the o-mode which is approximately valid under typical coronal conditions. We note that in general the o-mode emissivity is smaller (Dulk & Marsh 1982); we thus overestimate η somewhat, and hence we will underestimate the total energy content in the electrons accordingly. Since most of the emission is radiated by electrons with large pitch angles, we set $\theta = 60^\circ$ in what follows. This represents an average for a uniform pitch angle distribution with δ around 3 in equation 4. The radio flux then is

$$f_R(t) = \frac{\eta V(t)}{d^2} = \frac{f(B, \delta, \nu)}{d^2} N(t) V(t) \quad (5)$$

where V is the source volume, d is the distance to the source, and $f(B, \delta, \nu)$ collects various terms from equation 4. The total instantaneous kinetic energy in the electron distribution (given in equation 3) is

$$\begin{aligned} E_{\text{kin}}(t) &= N(t) V(t) (\delta - 1) E_0^{\delta-1} \int_{E_0}^{\infty} E^{-(\delta-1)} dE \\ &= N(t) V(t) \frac{\delta - 1}{\delta - 2} E_0 \end{aligned} \quad (6)$$

where $\delta > 2$ has been assumed. The expression $N(t) V(t)$ is obtained from equation 5 with the known radio flux f_R . We finally need to specify values for δ and B . Our single-frequency observation is not sufficient to derive these values. However, from a large body of published modeling results, likely values are within the ranges $2.0 < \delta \leq 3.5$ and $20 \leq B \leq 200$ G (e.g., Mutel et al. 1985; Morris et al. 1990; Chiuderi Drago & Franciosini 1993; Jones et al. 1994). We consider the range $2.1 \leq \delta \leq 3.5$.

Travel times of electrons of 10–100 keV along a magnetic loop of 10^9 cm are of order 1 s, i.e., if the electrons all get lost in the deeper atmospheric layers, then equation 6 gives the energy that should be replaced every second. However, radio-emitting electrons are probably trapped in magnetic fields for some time by virtue of their large pitch angles, while a large fraction of the lower-energy electrons that carry most of the energy to heat the chromosphere arrive there earlier.

The decay time τ cannot exceed the synchrotron loss time τ_s ,

$$\tau_s = \frac{6.8 \times 10^8}{B^2 \gamma} \quad [\text{s}] \quad (7)$$

(Petrosian 1985), where γ is the Lorentz factor of the electrons. For electrons observed at a frequency ν ,

$$\nu \approx \gamma^2 \nu_B. \quad (8)$$

Substituting ν_B and inserting γ into equation 7 leads to

$$\tau_s = \frac{1.1 \times 10^{12}}{B^{3/2} \nu^{1/2}} \quad [\text{s}]. \quad (9)$$

For our ranges of B , τ_s is minimized for $B = 200$ G, $\tau_s = 5500$ s. However, the fastest observed decay times in the radio light curve are of order 2000 s and possibly as small as 1000 s. We conclude that, in the framework of our simplistic model, losses other than synchrotron losses (most likely scattering into the loss cone and precipitation into the chromosphere, possibly also collisional losses) predominate. We henceforth adopt an upper limit to the lifetime of radio-emitting electrons of $\tau = 1500$ s.

The total energy injection rate is thus overestimated from the radio information. Starting at time $t = 0$ and assuming that the complete particle distribution ‘decays’ independently of energy by continuously losing energy (by various processes as mentioned above) and thus eventually thermalizing, the instantaneous number of radio-emitting particles evolves as

$$N(t)V(t) = N(0)V(0)e^{-t/\tau} + \int_0^t \frac{d[N_+(t')V(t')]}{dt'} e^{-(t-t')/\tau} dt' \quad (10)$$

where $d[N_+V]/dt \geq 0$ is the injection rate of new electrons. The first term on the right-hand side describes the decaying density of particles already present at $t = 0$, while the second term describes the evolution of newly injected electrons.

We note that equation 10 implies a convolution of the electron injection rate with a cut-off exponential function. The injection rate should thus peak considerably before the observed peak of $f_R \propto N(t)V(t)$ if τ were large. We take the very close temporal coincidence between the radio light curve and the derivative of the X-ray light curve as further a-posteriori support for a small energy loss time for the high-energy electrons. For $\tau = 1000$ s, the time delay between peak injection rate and peak $N(t)V(t)$ is negligible, while for $\tau = 1500$ s, it amounts to about 1000 s, which is still rather small. Equation 10 implies

$$\frac{d[N_+(t)V(t)]}{dt} = \frac{d[N(t)V(t)]}{dt} + \frac{N(t)V(t)}{\tau}. \quad (11)$$

In what follows, we subtract the apparently quiescent emission level of 3 mJy from the radio light curve (Figure 1c). The expression involving $N(0)$ in equation 10 can therefore be neglected, also because of the rather rapid decay time. It is easy to show that the rate of electron injection $d[N_+V]/dt$ is positive at a given time t if the observed decay time scale of

$f_R(t) \propto N(t)V(t)$ is larger than the assumed intrinsic decay time τ of the electron population. Since the latter is a necessary condition, we fulfil $d[N_+V]/dt > 0$ by adopting a value for τ at the lower limit of the measured decay time scales in the radio light curve, as done above.

When the rate of change in the derived instantaneous energetic-particle number $N(t)V(t)$ is small (first term on the right-hand side of equation 11, e.g., around the radio peak time), then the injection rate of particles is equal to $N(t)V(t)/\tau$, and the injected power analogously equals the total energy content divided by τ . The total number of injected electrons can be obtained by integrating equation 11 in time across the complete radio flare (time interval $[T_0, T] = [1.03, 1.32]$ d). Since the radio light curve approximately returns to the pre-flare level, $N(t)V(t)$ in equation 5 returns to the same value; thus, the first term in equation 11 does not contribute to the integral, and the total number of injected electrons is

$$\begin{aligned} \mathcal{N} &= \frac{1}{\tau} \int_{T_0}^T N(t)V(t)dt \\ &= 1.55 \times 10^{19} 10^{3.49\delta} B^{0.22-0.90\delta} \frac{d^2}{\tau} \int_{T_0}^T f_R(t)dt. \end{aligned} \quad (12)$$

The total injected energy can then be obtained from $\mathcal{E} = \mathcal{N}E_0(\delta-1)/(\delta-2)$ (equivalent to equation 6). We have performed the integration 12 for the B and δ values allowed here. The result is graphically shown in Figure 2. For the selected parameter range, the total injected energy is of order $10^{33} - 10^{36}$ erg. We compare this energy with the total energy loss in the second X-ray flare after 1.03 d. Judged from the count rate, the excess luminosity above the slow decay from the first flare peak reaches $\approx 3 \times 10^{30}$ erg s $^{-1}$. With a half-duration of about 0.15 d, we obtain a total radiated energy of 4×10^{34} erg. This value compares favorably with the estimates in Figure 2. While there is no proof for a causal relation between high-energy electrons and coronal heating, the energy budget is compatible with such a scenario for a reasonable range of parameters B, δ .

5. Conclusions

We note that, within the framework of our simplified model assumptions, our energy estimate is conservative. The lifetime τ of the non-thermal electron population has been adopted at the highest possible value compatible with the radio light curve (i.e., approximately equal to the shortest decay time scale in the observed radio emission). Equation 12 shows that a shorter possible lifetime requires a proportionately larger total energy input. In that case, the light curve variability is controlled by the time scales of the particle accelerator. If electrons get lost after one magnetic-loop crossing time, then $\tau \approx$ a few seconds for typical loop sizes, and the rapid replenishment of electrons requires an energy input into

the system up to 3 orders of magnitude higher than estimated above. We conclude that not only does the relative timing between radio and X-ray emissions support the chromospheric evaporation scenario, but the total energy content in the injected high-energy electrons could easily satisfy or largely exceed the requirements set by the observed X-ray losses.

The observation described here provides strong support for the chromospheric evaporation scenario in a star that may maintain a corona considerably different from the Sun's (e.g., containing much larger magnetic loops, confining much hotter and perhaps also denser thermal plasma, magnetic field lines that may be arranged in the form of large global dipoles, possibly also between the companion stars, etc). In retrospect, we find a similar timing between radio and X-ray flare events in some previously published light curves, although the Neupert effect was not discussed. Most evidently, radio emission peaking before the soft X-rays, thus suggesting the presence of a Neupert effect, can be seen in the examples presented by Vilhu et al. (1988), Stern et al. (1992), Brown et al. (1998), and Ayres et al. (2001). Clearly, differing behavior has been noted as well. First, the Sun shows the Neupert effect most reliably in the class of impulsive flares, whereas 50% of all gradual flares, often related to energy release at high coronal altitudes, show a different behavior (Dennis & Zarro 1993). It is possible that the connectivity of magnetic fields between the high corona and the chromospheric regions is different in these cases, impeding the free flow of electrons and consequent chromospheric evaporation. Thermalization of fast electrons could also occur in the corona already if the travel distances are long enough and the densities high enough. Stellar counter-examples of the Neupert effect include an impulsive optical flare with following gradual radio emission (van den Oord et al. 1996), gyrosynchrotron emission that peaks after the soft X-rays (Osten et al. 2000), and an X-ray depression during strong radio flaring (Güdel et al. 1998). Note also that complete absence of correlated flaring has been observed at radio and UV wavelengths (e.g., Lang & Willson 1988).

Evidence for chromospheric evaporation in an RS CVn binary system is potentially important to understand to what degree the solar analogy can be applied to such stellar systems. Although magnetospheric sizes as measured in radio waves are several times larger than the Sun, VLBI observations have suggested that flares start out in compact, unresolved cores that are well localized in magnetic active regions close to the stellar surface (Mutel et al. 1985). Our observations of a Neupert effect strongly suggest solar analogy in the physics of energy release and transport in this binary system, at least for the large flare reported here.

We acknowledge the hospitality of CASA/University of Colorado where most of this paper was written. Research at PSI has been supported by the Swiss National Science Foundation (grant 2100-049343). SRON is supported financially by NWO. The present

project is based on observations obtained with *XMM-Newton*, an ESA science mission with instruments and contributions directly funded by ESA Member States and the USA (NASA). The VLA is a facility of the National Radio Astronomy Observatory, which is operated by Associated Universities, Inc., under cooperative agreement with the National Science Foundation.

REFERENCES

Ayres, T. R., Brown, A., Osten, R. A., Huenemoerder, D. P., Drake, J. J., et al. 2001, *ApJ*, 549, 554

Bastian, T. S., Benz, A. O., & Gary, D. E. 1998, *ARA&A*, 36, 131

Beasley, A. J., et al. 2002, in preparation

Brown, A., Osten, R. A., Drake, S. A., Jones, K. L., & Stern, R. A. 1998, In The Hot Universe. IAU Symp 188, Eds. K Koyama, S. Kitamoto, & M. Itoh (Dordrecht: Kluwer), 215

Chiuderi Drago, F., & Franciosini, E. 1993, *ApJ*, 410, 301

Dennis, B. R. 1988, *Solar Phys.*, 118, 49

Dennis, B. R., & Zarro, D. M. 1993, *Solar Phys.*, 146, 177

Drake, S. A., Simon, T., & Linsky, J. L. 1989, *ApJ*, 71, 905

Dulk, G. A., & Marsh, K. A. 1982, *ApJ*, 259, 350

Engvold, O., et al. 1988, *A&A*, 192, 234

ESA 1997, The Hipparcos and Tycho Catalogues, ESA SP-1200

Feldman, P. A., Taylor, A. R., Gregory, P. C., Seaquist, E. R., Balonek, T. J., Cohen, N. L. 1978, *AJ*, 83, 1471

Güdel, M., Benz, A. O., Schmitt, J. H. M. M., & Skinner S. L. 1996, *ApJ*, 471, 1002

Güdel, M., Guinan, E. F., Etzel, P. B., Mewe, R., Kaastra, J. S., & Skinner, S. L. 1998, In 10th Cambridge Workshop on Cool Stars, Stellar Systems, and the Sun, ed. R. Donahue & J. A Bookbinder, (San Francisco: ASP), 1247

Hawley, S. L., et al. 1995, *ApJ*, 453, 464

Hudson, H., & Ryan, J. 1995, *ARA&A*, 33, 239

Jansen, F., et al. 2001, *A&A*, 365, L1

Jones, K. L., Stewart, R. T., Nelson, G. J., Duncan, A. R. 1994, *MNRAS*, 269, 1145

Jones, K. L., Brown, A., Stewart, R. T., & Slee, O. B. 1996, *MNRAS*, 283, 1331

Lang, K. R., & Willson, R. F. 1988, *ApJ*, 328, 610

Morris, D. H., Mutel, R. L., & Su, B. 1990, *ApJ*, 362, 299

Mutel, R. L., Lestrade, J.-F., Preston, R. A., & Phillips, R. B. 1985, *ApJ*, 289, 262

Neupert, W. M. 1968, *ApJ*, 153, L59

Osten, R. A., & Brown, A. 1999, *ApJ*, 515, 746

Osten, R. A., Brown, A., Ayres, T. R., Linsky, J. L., Drake, S. A., Gagné, M., Stern, R. A. 2000, *ApJ*, 544, 953

Pallavicini, R., Willson, R. F., & Lang, K. R. 1985, *A&A*, 149, 95

Petrosian, V. 1985, *ApJ*, 299, 887

Sakao, T. 1994, Characteristics of solar flare hard X-ray sources as revealed with the hard X-ray telescope aboard the Yohkoh satellite. PhD thesis. (Tokyo: University of Tokyo).

Schrijver, C. J., Mewe, R., van den Oord, G. H. J., & Kaastra, J. S. 1995, *A&A*, 302, 438

Singh, K. P., Slijkhuis, S., Westergaard, N. J., Schnopper, H. W., Elgaroy, O., Engvold, O., & Joras, P. 1987, *MNRAS*, 224, 481

Stern, R. A., Uchida, Y., Walter, F. M., Vilhu, O., Hannikainen, D., Brown, A., Vealé, A., & Haisch, B. M. 1992, *ApJ*, 391, 760

Strassmeier, K. G., Hall, D. S., Fekel, F. C., & Scheck, M. 1993, *A&AS*, 100, 173

Strüder, L., et al. 2001, *A&A*, 365, L7

van den Oord, G. H. J., Doyle, J. G., Rodonò, M., Gary, D. E., Henry, G. W., et al. 1996, *A&A*, 310, 908

Vilhu, O., Caillault, J.-P., & Heise, J. 1988, *ApJ*, 330, 922

White, S. M., & Franciosini, E. 1995, *ApJ*, 444, 342

Yi, Z., Elgaroy, O., Engvold, O., & Westergaard, N. J. 1997, A&A, 318, 791

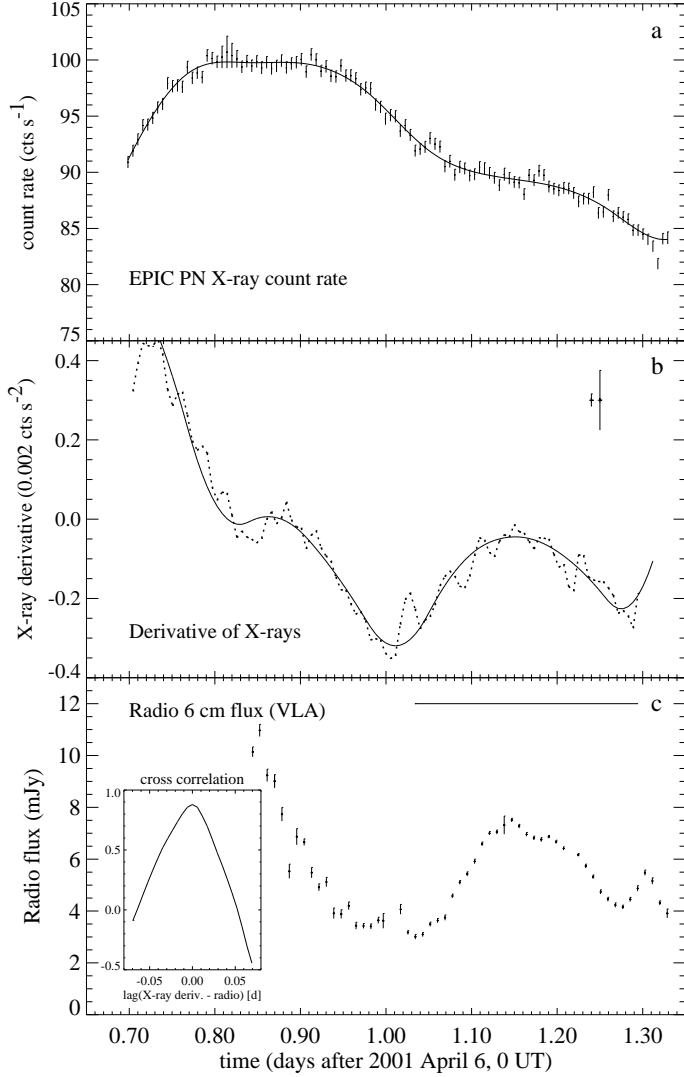


Fig. 1.— Light curves of σ Gem. **a)** (top): *XMM-Newton* EPIC PN light curve, binned to 500 s and corrected for dead time. The smooth solid curve has been obtained from a Chebychev polynomial fit of order 9. **b)** (middle): The time derivative of the smoothed X-ray light curve. The solid curve shows the time derivative of the Chebychev polynomial fit above; the dotted curve was derived from a boxcar-smoothed light curve (boxcar length = 11; not shown). For the latter derivative, the larger error bar in the upper right corner illustrates the absolute uncertainty for any single derivative, whereas the smaller error bar indicates the relative scatter between nearest neighbors and is smaller due to correlations introduced by the smoothing. **c)** (bottom): The VLA 6 cm light curve, binned to \sim 750 s (observing scan length). The inset shows the cross-correlation function of the radio light curve and the X-ray time derivative, computed for the time interval marked with a horizontal bar above the second radio flare.

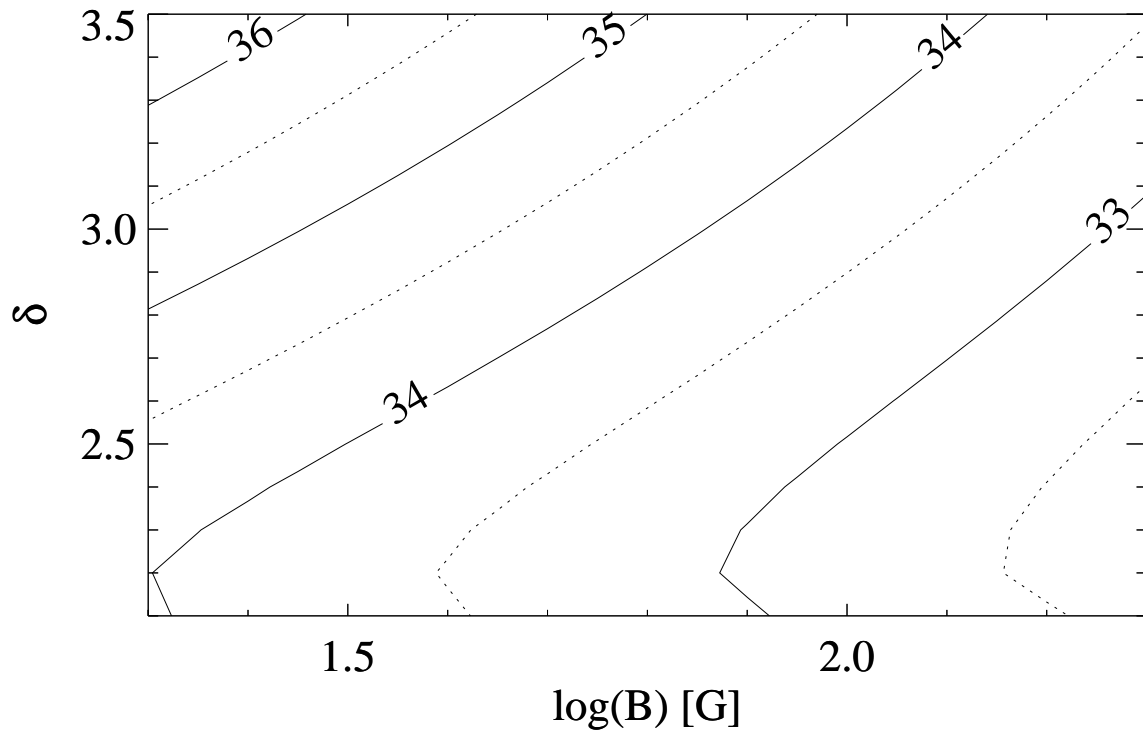


Fig. 2.— Estimated kinetic energies E in accelerated electrons (above 10 keV), integrated over the complete second radio flare, as a function of the magnetic field strength and the power-law index δ . Solid contours are labeled with $\log E$, and dashed contours refer to half-decade $\log E$ values ($\log E = 32.5$ etc).